

# Noise-driven Topological Changes in Chaotic Dynamics

Gisela D. Charó,<sup>1,2,a)</sup> Mickaël D. Chekroun,<sup>3</sup> Denisse Sciamarella,<sup>4</sup> and Michael Ghil<sup>5,6</sup>

<sup>1)</sup>Centro de Investigaciones del Mar y la Atmósfera, Facultad de Ciencias Exactas y Naturales, Universidad de Buenos Aires, C1428EGA CABA, Argentina.

<sup>2)</sup>Institut Franco-Argentin d'Études sur le Climat et ses Impacts (IFAECI), UMI 3351 (CNRS-CONICET-UBA), C1428EGA CABA, Argentina.

<sup>3)</sup>Weizmann Institute of Science, Rehovot, Israel.

<sup>4)</sup>Institut Franco-Argentin d'Études sur le Climat et ses Impacts (IFAECI), UMI 3351 (CNRS-CONICET-UBA), C1428EGA CABA, Argentina.

<sup>5)</sup>Department of Atmospheric & Oceanic Sciences, University of California, Los Angeles, CA 90095-1565, USA

<sup>6)</sup>Geosciences Department and Laboratoire de Météorologie Dynamique (CNRS and IPSL), École Normale Supérieure and PSL University, 75231 Paris Cedex 05, France

(Dated: 25 April 2022)

Noise modifies the behavior of chaotic systems. Algebraic topology sheds light on the most fundamental effects involved, as illustrated herein by using the Lorenz (1963) model. This model's deterministic attractor is “strange” but frozen in time. When driven by multiplicative noise, the Lorenz model's random attractor (LORA) evolves in time. Here, we use Branched Manifold Analysis through Homologies (BraMAH) to describe changes in LORA's coarse-grained topology. BraMAH is thus extended from deterministic flows to noise-driven systems. LORA's homology groups and branched manifold differ from the deterministic ones and they change in time.

**Henri Poincaré first described the way in which a dynamical system's properties depend upon its topology. The advantage of using topology instead of geometry or fractality to describe chaotic data lies in the fact that topology provides information about the stretching, folding, tearing and squeezing mechanisms that act in phase space to shape the flow. R. F. Williams introduced the concept of branched manifold to characterize the surface of the Lorenz attractor<sup>1</sup> and, with J. Birman<sup>2</sup>, used it to classify chaotic attractors in terms of the way in which their branches are knotted. This description goes beyond merely counting the branches: their organization and the presence of half-twists in some of them is highly relevant. These features can be captured without dimensionality restrictions using homologies<sup>3</sup>. Here, we extend the usage of branched manifolds beyond the deterministic framework by investigating the evolution in time of the topological structure of the Lorenz Random Attractor (LORA)<sup>4</sup>. LORA's branched manifold is found to undergo abrupt changes for some values of the noise forcing, suggesting that the effects of noise on chaotic dynamics can be robustly addressed in this manner. Topological tipping points can thus be understood as abrupt changes in the topological description of a random attractor's branched manifold.**

## I. INTRODUCTION AND MOTIVATION

The use of topological concepts to describe complex physics goes back at least to Lord Kelvin, who proposed that atoms were knotted vortices swirling in the æther, an invisible

medium believed at that time to fill the surrounding space<sup>5</sup>. Though incorrect, Kelvin's vision stimulated active research in knot theory<sup>6,7</sup> and eventually led to the awareness that knots and related tangled structures do actually form in various physical phenomena and can have a pivotal, albeit still poorly understood influence on turbulent fluid dynamics<sup>8,9</sup>, quantum field theory<sup>10</sup>, and magnetic fields<sup>11,12</sup>, to cite but a few areas of physics. In his seminal work, Moffatt<sup>13</sup> showed that helicity measures the total knottedness and linkage of a flow and that it is an invariant in ideal, viscosity-lacking fluids, like liquid helium. In viscous fluids, helicity fluctuates, and knots can experience transformations or unravel<sup>14</sup>.

In dissipative chaotic dynamical systems, applications of algebraic topology<sup>15</sup>, which studies algebraic invariants that classify topological spaces up to homeomorphism<sup>16</sup>, have also attracted much attention over the past three decades<sup>17–19</sup>. Branched manifolds<sup>2,20</sup>, in particular, have played a central role in the characterization of the coarse-grained features of chaotic dynamics. These objects provide a simple but powerful “cartoon” of the stretching and folding responsible for the creation of strange attractors, and are also referred to as a template or a knot holder. In the present paper, we wish to extend the usefulness of branched manifolds to chaotic systems with time-dependent forcing, in particular to noise-driven ones.

Interest in such nonautonomous and random dynamical systems (NDSs and RDSs) has been greatly stimulated recently by the effects of anthropogenic forcing on the climate system, on the one hand, and by the multiscale character of the system's intrinsic variability, on the other<sup>21,22</sup>. The latter problem has been addressed by stochastic parameterizations of unresolved scales in high-order models and has led to more realistic low-order models; see<sup>23–26</sup> and references therein.

With this motivation in mind, Chekroun, Simonnet, and Ghil<sup>4</sup> studied interactions between noise and nonlinear effects from a qualitative dynamical viewpoint, through high-resolution numerical computations. The pullback attractors

<sup>a)</sup>Electronic mail: [gisela.charo@cima.fcen.uba.ar](mailto:gisela.charo@cima.fcen.uba.ar)

(PBAs) of RDS theory<sup>27,28</sup> provide the appropriate framework for doing so and are the mathematically rigorous counterpart of the heuristically defined snapshot attractors of nonlinear physics<sup>29</sup>. Further theoretical details on PBAs and RDSs appear in Appendices A and B.

In the random, RDS setting, a PBA is computed by following an ensemble of trajectories, each driven by the same noise path. This way, the well-known smoothing effect of noise due to a single very long integration of the stochastic system disappears in the pullback approach and the fractal structure of the chaotic dynamics is fully captured when the unperturbed nonlinear system's dynamics is itself chaotic.

PBAs thus provide the perfect way to reveal the time-dependent stretching and folding caused by the interactions between noise and chaotic nonlinearity. In their study of the stochastic Lorenz<sup>30</sup> model's PBA, dubbed LORA, ref<sup>4</sup> pointed out that the stretch-and-fold mechanisms give rise to three distinct components of the flow in phase space: a smooth evolution tied to the Lorenz model's deterministic convection; a pervasive, local "jiggling" due to the roughness of the driving multiplicative noise; and sudden deformations of the random PBA's overall support. The static picture of the strange attractor generated by deterministic chaos<sup>31,32</sup> is thus replaced, in the presence of noise, by a dynamic version that is even stranger, and that we will refer to as *noise-driven chaos* in what follows.

Noise-driven chaos offers therewith a natural framework for extending the concepts and tools of chaos topology towards more realistic situations in fluid dynamics, the climate sciences and elsewhere, to advance the understanding of complex nonlinear dynamics in the presence of noise. The purpose of this article is to examine noise-driven chaos through the lens provided by algebraic-topology tools.

To do so, we study here LORA's changes in time by applying a relatively recent Topological Data Analysis (TDA) methodology, called Branched Manifold Analysis through Homologies (BraMAH)<sup>33</sup>. TDA is widely used nowadays to examine the shape and structure of large, but mostly stationary data sets by focusing on their connectivity<sup>34–36</sup>.

A chaotic system's time-evolving branched manifold is defined here locally as an integer-dimensional set in phase space that is the robust skeleton of the point cloud associated, at each instant, with the invariant measure supported by LORA; see Appendix C for the theoretical underpinnings of the latter. The point cloud in BraMAH is first decomposed into subsets of points, called cells that are glued together into a cell complex, the coarse skeleton of the structure upon which the point cloud lies. The cell complex construction method is designed to approximate a point cloud lying on a branched manifold. Therefore, the topological features of the cell complex will unveil the topological signature of the branched manifold. BraMAH is briefly recalled and refined in the next section and Appendix D provides further details.

The numerical results and their robustness are described in Sect. III. The key results are:

- (a) the BraMAH methodology captures LORA's time-evolving topological structure well by constructing this manifold at each instant in time;
- (b) this structure differs from that obtained for the deterministic

Lorenz model's strange attractor; and

- (c) the noise-driven model's otherwise slowly evolving structure exhibits apparently sharp transitions in time.

These results are briefly discussed in Sect IV.

## II. BRANCHED MANIFOLD ANALYSIS THROUGH HOMOLOGIES (BRAMAH)

Pursuing our goal of examining noise-driven chaos through the lens of algebraic-topology tools, we first provide some background on TDA in general and on BraMAH in particular. This background is followed by a more detailed presentation of the BraMAH methodology itself.

### A. Background on TDA and BraMAH

TDA relies on recent computational advances, including homology computation from point clouds, to study the shape and structure of large data sets by focusing on their connectivity<sup>34–36</sup>; it is used more and more in numerous and diverse research areas, including image processing<sup>37</sup>, the spread of social and biological contagions on networks<sup>38</sup>, percolation theory<sup>39</sup>, genomics and evolutionary dynamics<sup>40,41</sup>, and protein structure<sup>42</sup>.

Key developments in TDA include the computation of Persistence Homologies (PHs)<sup>43,44</sup>, which use a parameter to construct a family of nested cell complexes that monitor the "lifetime" of basic topological features in a point cloud, such as its holes. PHs were applied to shed further light on the strange attractor of the Lorenz system<sup>45</sup>, among other well-known deterministically chaotic systems. In E.N. Lorenz's own terms<sup>30</sup>, the flow on the attractor's "surface" passes "back and forth from one spiral to the other without intersecting itself." This surface is topologically equivalent to what is now called a branched manifold<sup>46</sup>.

Recently, Strommen *et al.*<sup>47</sup> have adapted PHs to yield a computationally tractable identification and classification of multiple weather regimes<sup>32,48–50</sup> on the basis of the topological structure of the atmospheric flow in a low-dimensional, high-variance subspace of a given data set. Given the large number of classification schemes — based on phase space clustering and temporal-persistence criteria, among others<sup>51,52</sup> — such a topological approach could provide additional insights into the still poorly understood mechanisms of the complex organization of the atmosphere's "regime diagram"<sup>53</sup>.

BraMAH<sup>3,33,54</sup> is a TDA method originally devised to study the phase space topology of point clouds generated by deterministic nonlinear dynamical systems. These clouds may represent chaotic attractors, invariant manifolds, and also semi-flows on a broader class of objects that are neither attractors nor manifolds<sup>19</sup>. The method's specificities hinge on the cell complex construction rules, as well as on the way it extracts the topological properties associated with the complexes so constructed.

The manner in which BraMAH constructs a cell complex differs from other TDA construction methods — such as the

Čech or Vietoris-Rips methods<sup>43,55</sup> — in its using explicitly the fact that the point cloud under study lies on a branched manifold. This property of the dynamics generating the point cloud is used to produce a BraMAH cell complex, i.e. a complex in which each cell represents a large subset of points that jointly approximate a locally Euclidean set, whose dimension respects the local dimension of the branched manifold. The output contains all the information that is needed to identify the organization and connectivity of the branches. Some of the branches may have torsions that are important for the correct identification of an attractor; hence BraMAH also distinguishes, for instance, a standard strip from a Möbius strip.

## B. The BraMAH Methodology

Sciamarella and Mindlin<sup>3,33</sup> formulated the BraMAH method and used it to extract the topological structure of deterministically chaotic flows from time series. To do so, one embeds the time series in a suitable phase space in order to generate a point cloud. Dynamically generated point clouds are well described by a branched manifold<sup>18</sup>. BraMAH has been applied so far to speech data<sup>3</sup>, to slow-fast systems<sup>20,33,56</sup>, and to Lagrangian dynamics in fluid flows<sup>54</sup>. Here it is being applied for the first time to data sets generated by noise-driven chaos. The methodology requires approximating the structure of the branched manifold that supports the point cloud by a cell complex, as defined in algebraic topology<sup>57</sup>. The structure of this invariant manifold can be approximated with “building blocks.” In algebraic topology, these building blocks are Euclidean closed sets (segments, disks, etc.), called  $n$ -cells, where  $n \in \mathbb{N}_0$ . A point is a 0-cell, a line segment joining two points is a 1-cell, a polygon is a 2-cell and so forth. Constructing and assembling these cells according to the BraMAH rules detailed in Appendix D builds a cell complex that is the branched manifold’s skeleton.

The topological structure of this cell complex is studied by using homology groups<sup>57</sup> and orientability chains<sup>3</sup>. The homology groups  $H_k$  identify the  $k$ -dimensional holes ( $k$ -holes) of a topological space of dimension  $n$ , where  $k \in \mathbb{N}_0$  and  $k \leq n$ . The group  $H_0$  identifies the connected components (0-holes),  $H_1$  the cycles (1-holes),  $H_2$  the cavities (2-holes), and if  $k \geq 2$ ,  $H_k$  the hypercavities ( $k$ -holes). By construction, a BraMAH cell complex is uniformly oriented. The orientability chain indicates the number and location of torsions in the cell complex. For further details of the BraMAH method, see Appendix D.

When evaluating a time-dependent structure like LORA, one has to ask whether its topology is time-dependent. In order to answer this question, we take two steps: (1) generate the point clouds that approximate LORA at successive time instants, called “snapshots”<sup>4,58,59</sup>, and (2) compute the topological properties associated with each snapshot using BraMAH.

In step (1), the point cloud approximating LORA is generated by solutions of the stochastic Lorenz model (SLM) introduced by Chekroun, Simonnet, and Ghil<sup>4</sup>. In SLM, the equations of the classical Lorenz<sup>30</sup> deterministic model are perturbed by a multiplicative noise in the Itô sense<sup>28</sup>, with  $W_t$

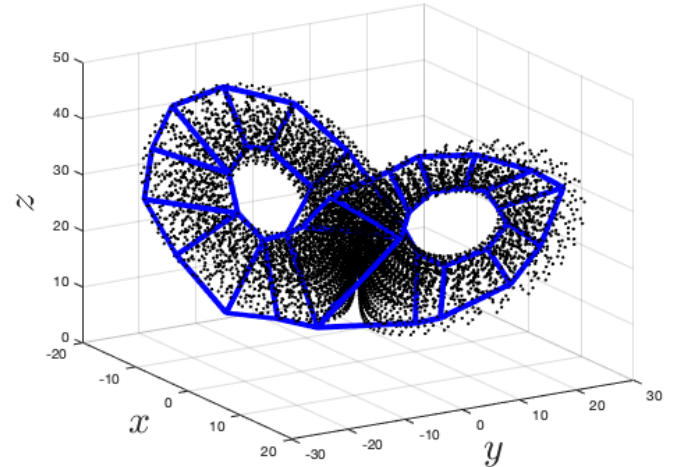


FIG. 1. Point cloud (in black) juxtaposed on the cell complex (blue borders) obtained by BraMAH for the deterministic Lorenz<sup>30</sup> attractor, with  $\sigma = 0$  in Eq. (1).

a Wiener process and  $\sigma > 0$  the noise intensity:

$$\begin{aligned} dx &= s(y - x)dt + \sigma x dW_t, \\ dy &= (rx - y - xz)dt + \sigma y dW_t, \\ dz &= (-bz + xy)dt + \sigma z dW_t; \end{aligned} \quad (1)$$

here  $r = 28$ ,  $s = 10$ ,  $b = 8/3$  are the standard parameter values for deterministically chaotic behavior.

The time-dependent sample measures  $\mu_t$  associated with the SLM system (1) are probability measures for the population density of any ensemble of initial data driven by the same noise realization until time  $t$ , after removal of the transient behavior. Mathematically, these measures are of Sinai-Ruelle-Bowen (SRB) type<sup>60–62</sup>, i.e., they are supported by the foliation of unstable manifolds that structure the random attractor<sup>4</sup>.

A numerical estimation  $\hat{\mu}_t$  of such a measure can be computed at any time instant  $t$  by a pullback approach, i.e., by letting a large set of  $N_0$  initial points  $\{\mathbf{x}_j(0) = (x_j, y_j, z_j)(t = 0) : j = 1, \dots, N_0\}$  “flow” in phase space from the remote past until time  $t$ , for a fixed noise realization  $\omega$ . The convergence of the sample measure’s approximation  $\hat{\mu}_t = \hat{\mu}_t(N_0)$  is studied as the number  $N_0$  of initial points increases; it is observed herein for  $N_0 \simeq 10^8$ .

Each point within a given cloud at time  $t$  is mapped to a value of  $\hat{\mu}_t$  that is obtained by averaging over a volume surrounding that point: higher or lower  $\hat{\mu}_t$ -values correspond to more or less populated regions of the random attractor. We wish to characterize the topology of the point cloud’s most populated regions but also to ascertain this topology’s robustness and perdurance as  $N_0$  changes. In order to do this, a threshold  $\bar{n}$  for  $\hat{\mu}_t$  must be selected, as discussed below.

## III. RESULTS

For starters, we provide a BraMAH analysis of the classical Lorenz<sup>30</sup> attractor, with  $\sigma = 0$  in Eq. (1). The strange attractor and the BraMAH cell complex associated with its branched

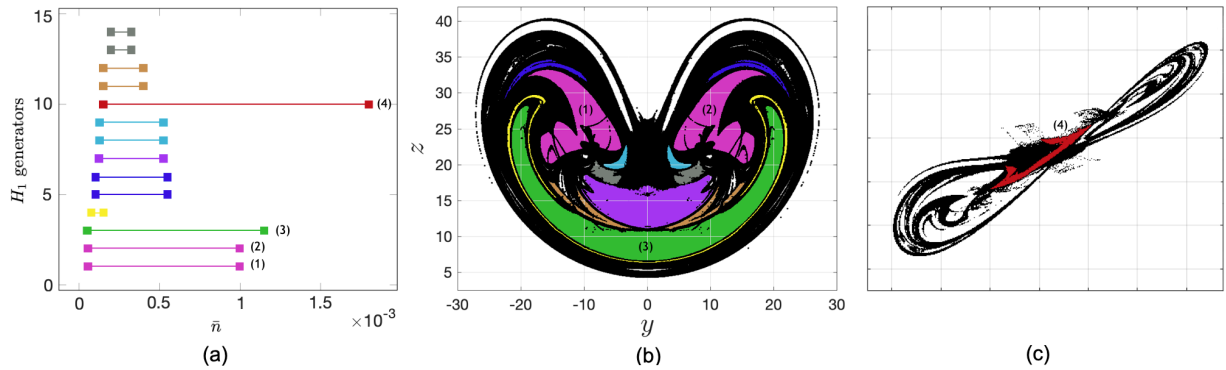


FIG. 2. LORA snapshot at  $t = 40.27$ , for  $\sigma = 0.3$ . (a) perdurance of the 1-holes as the density threshold  $\bar{n}$  is increased; the most perdurant holes are labeled with numbers (1)–(4); (b)  $(y, z)$  projection of the sieved point cloud ( $\bar{n} = 2 \times 10^{-4}$ ) with 13 colored 1-holes; (c) projection onto the plane  $-2.25x - 20y + 6z = 0$  of the sieved point cloud with the 1-hole labeled (4) in red.

manifold is shown in Figure 1. The cell complex presents one connected component, i.e.,  $H_0 \sim \mathbb{Z}$ , and two homologically independent 1-holes associated with each wing of the butterfly, i.e.,  $H_1 \sim \mathbb{Z}^2$ ; there are no torsions, i.e.,  $O_1 \sim \emptyset$ , and no enclosed cavities, i.e.,  $H_2 \sim \emptyset$ .

Solutions of the SLM generate data sets in the form of 3-dimensional point clouds  $\{\mathbf{x}_i \in \mathbb{R}^3 : 1 \leq i \leq N_0\}$  with  $N_0 = 10^8$ . These point clouds are sieved using a threshold value  $\bar{n}$  in the sample measure  $\hat{\mu}_t$  in order to keep only those points that correspond to the most populated regions of the cloud. For each  $\bar{n}$ -value, a point cloud  $\{\mathbf{x}_i : \hat{\mu}_t(\mathbf{x}_i) \geq \bar{n}\}$  is used to construct one BraMAH cell complex.

At  $t = 40.27$ , there are only four 1-holes that perdure as the value  $\bar{n}$  of the threshold increases. Notice that such a perdurance plot should not be read as a PH barcode: at each  $\bar{n}$ -value, BraMAH uses a point cloud that differs in its size and elements to construct the cell complex, whereas in PHs there is a single point cloud under consideration and the horizontal axis sweeps a parameter value that regulates the construction of nested cell complexes for the same point cloud.

The sieved point cloud used in Figures 2(b) and (c) is constructed using  $\bar{n} = 2 \times 10^{-4}$  as threshold value for the estimated sample measure  $\hat{\mu}_t$ : Figure 2(b) shows the projection of the sieved point cloud onto the  $(y, z)$ -plane, with thirteen 1-holes colored and three of them labeled with the numbers (1), (2) and (3). Panel (c) shows a 3-dimensional view of the sieved point cloud with the perdurant 1-hole labeled with number (4) in red. The colors of the holes correspond to those of the bars in Fig. 2(a). We analyze here the topology of successive LORA snapshots with noise intensity  $\sigma = 0.3$ .

The local dimension of the branched manifold is the same as in the deterministic case: locally, LORA remains a 2-branched manifold and no torsions are ever observed, i.e.,  $O_1 \sim \emptyset$ . Noise adds neither connected components nor cavities to the manifold, so that the groups  $H_0 \sim \mathbb{Z}$  and  $H_2 \sim \emptyset$  are the same as in Figure 1. The topological distinctions between LORA and the classical Lorenz<sup>30</sup> attractor are thus solely present in  $H_1$ . One notices immediately, though, that the number of 1-holes changes from one snapshot to another, with holes created or destroyed by the noise in the course of time.

This situation is illustrated in Figure 3 for three successive snapshots, at  $t = 40.09, 40.18$  and  $40.27$ ; for each snapshot,

we selected a threshold value  $\bar{n}$  at which the most perdurant 1-holes occur. The sieved point clouds are given in the 3 top panels, while the corresponding cell complexes are presented in the 3 bottom panels. The number of 1-holes undergoes large changes from one snapshot to the next, as suggested by the LORA video in the Supplementary Material of ref<sup>4</sup>.

#### IV. CONCLUDING REMARKS

We have topologically analyzed here a paradigmatic random attractor<sup>4</sup> associated with the Lorenz<sup>30</sup> convection model. The branched manifold constructed by BraMAH provides a coarse-grained skeleton of this attractor.

Our study shows a marked difference between the deterministic case and the noise-driven one. The stochastically perturbed system's random attractor, dubbed LORA, presents a much richer structure than the deterministic strange attractor, with a topology that also changes drastically in time. The framework introduced in this article to characterize such changes in topological features appears to hold promise for the understanding of topological tipping points (TTPs) in general.

A fairly straightforward BraMAH application to the climate sciences might clarify the following quandary of so-called subseasonal-to-seasonal (S2S) prediction<sup>63</sup>. The quandary deals with the role of intermittent vs. oscillatory low-frequency variability (LFV) in the atmosphere<sup>49,51</sup>. LFV refers to phenomena whose characteristic time of 10–100 days exceeds that of typical midlatitude storms of 5–7 days; see, for instance, Ghil and Childress<sup>32</sup>, Ch. 6.

Such phenomena include the so-called blocking of the westerlies and intraseasonal oscillations with periodicities of 40–50 days; the former is intermittent, or particle-like, the latter oscillatory or wave-like<sup>22,49</sup>. The quandary is which type of phenomenon dominates LFV and thus could contribute most to S2S prediction, cf. Ghil<sup>64</sup>, Fig. 1.

Blocking has been recently studied in Lucarini and Gritsun<sup>65</sup> by the unstable periodic orbits methodology of Gilmore<sup>18</sup>. It would appear that the BraMAH methodology proposed herein could address, more generally and efficiently, the waves-vs.-particles quandary of LFV and how it might be affected by global change<sup>64</sup>.

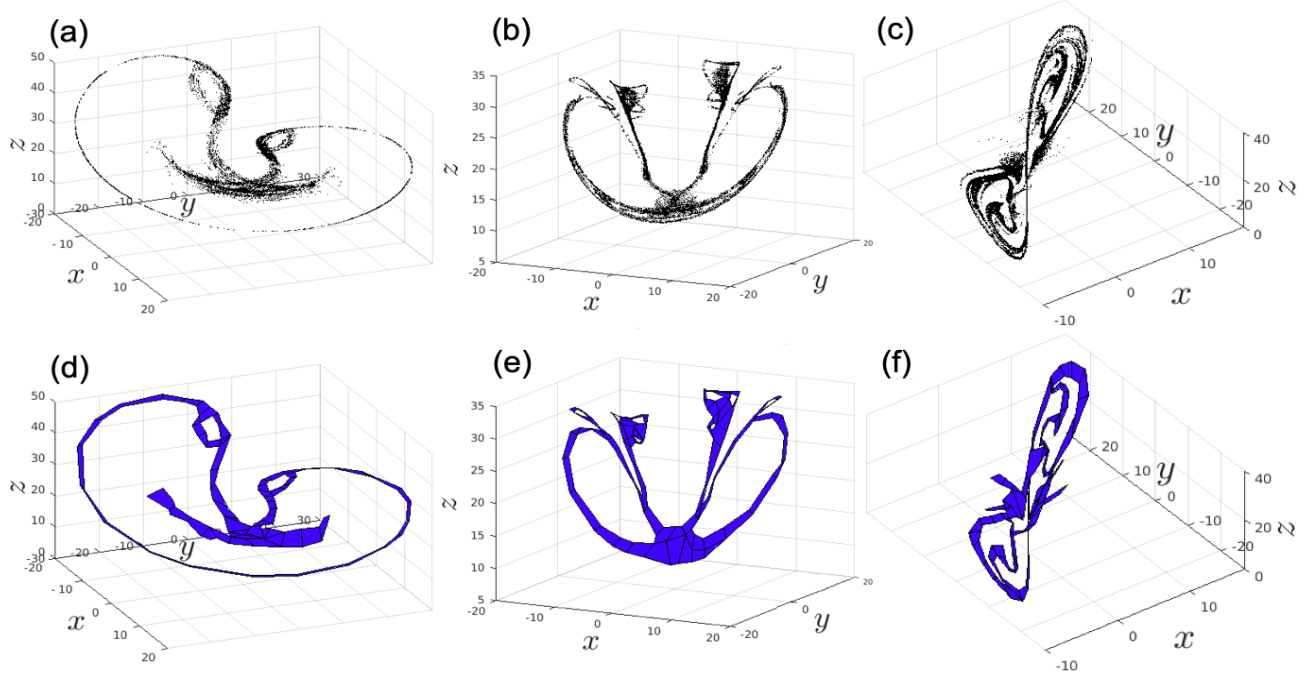


FIG. 3. Two representations of LORA snapshots with  $\sigma = 0.3$  and  $N_0 = 10^8$ : sieved point clouds (a)–(c) and cell complexes (d)–(f). (a,d)  $t = 40.09$ ,  $\bar{n} = 6 \times 10^{-4}$ ,  $H_1 \sim \mathbb{Z}^3$ ; (b,e)  $t = 40.18$ ,  $\bar{n} = 2.25 \times 10^{-3}$ ,  $H_1 \sim \mathbb{Z}^{10}$ ; and (c,f)  $t = 40.27$ ,  $\bar{n} = 7 \times 10^{-4}$ ,  $H_1 \sim \mathbb{Z}^4$ .

More broadly, tipping points have been given a precise definition in the climate sciences as a generalization to NDSs and RDSs of classical bifurcations in autonomous systems<sup>21,66</sup> and they are being actively pursued<sup>67–72</sup>. TTPs seem to be a further generalization of the concept that could help us apprehend sudden and drastic changes in time of model behavior, as well as drastic changes due to mean forcing intensity.

The gradual change of atmospheric concentrations of greenhouse gases and aerosols modifies global temperatures in a fairly smooth way<sup>73</sup>, as the case has been so far, although it might also lead to dynamical tipping points, as suggested by the above-cited papers. On the other hand, the intrinsic noise associated with cloud processes on small space and time scales affects the entire climate system through their interaction with dynamic and radiative processes on larger scales<sup>22</sup>.

This noise is considerably more complex than the one considered herein and the climate system is infinitely more complex than the Lorenz convection model we have studied. It is quite plausible, though, and certainly worth exploring further, whether such an interaction between more complex large-scale dynamics and more complex small-scale noise might not lead to striking surprises in not-too-distant times.

## ACKNOWLEDGMENTS

We thank many colleagues who asked good questions at several talks and posters given on this work; see, for instance, refs<sup>74,75</sup>. This work is supported by the French National program LEFE-NOISE (Les Enveloppes Fluides et l’Environnement) and by the CLIMAT-AMSUD 21-CLIMAT-05 project (D.S.). G.D.C. gratefully acknowledges her post-doctoral scholarship from CONICET and wishes to thank Juan Ruiz and the CIMA computing staff for support with the computations. This work was also partially supported by the European Research Council (ERC) under the European Union’s Horizon 2020 research and innovation program (grant agreement No. 810370), by a Ben May Center grant for theoretical and/or computational research and by the Israeli Council for Higher Education (CHE) via the Weizmann Data Science Research Center (M.D.C.). The article is TiPES contribution #46; this project has received funding from the European Union’s Horizon 2020 research and innovation program under grant agreement No. 820970 (M.G.).

## DATA AVAILABILITY

The data that support the findings of this study are available from the corresponding author upon request.

## Appendix A: PULLBACK ATTRACTORS

We summarize herein some pertinent facts on nonautonomous systems of ordinary differential equations,

$$\dot{x} = \mathbf{F}(t, x), \quad t \in \mathbb{R}, \quad (\text{A1})$$

## AUTHOR’S CONTRIBUTIONS

All authors contributed equally to this work.

considered in the framework of nonautonomous dynamical systems (NDSs);  $F$  denotes a smooth time-dependent vector field that governs the time evolution of the state  $x$  in a phase space  $X$ , taken for simplicity to be the Euclidean space  $\mathbb{R}^N$ .

Once existence and uniqueness are guaranteed, one can assign to this NDS a solution map  $\Phi(t, s)$ , which provides a two-time description of the motion: the time  $s$  when the system was initialized, and the time  $t \geq s$  of the system's current state. Thus

$$x(t) = \Phi(t, s)x_0$$

denotes the solution of Eq. (A1) at time  $t$ , when initialized at  $x(t) = x_0$  for time  $t = s$ . In the autonomous case, only the time interval  $t' = t - s$  separating  $s$  and  $t$  matters and  $\Phi(t, s)$  reduces to a standard flow  $\Phi(t')$ .

In the case of forced and dissipative systems, such as the climate system<sup>22,32</sup>, one can define a collection of subsets called a *pullback attractor* (PBA)<sup>4,28,70,76,77</sup>.

**Definition 1.** A PBA is a family  $\{\mathcal{A}(t)\}_{t \in \mathbb{R}}$ , where  $\mathcal{A}(t)$  is a compact subset of  $X$  at each time  $t$ . For each  $t \in \mathbb{R}$ , this family has two fundamental properties:

- (1) **Invariance:**  $\Phi(t, s)\mathcal{A}(s) = \mathcal{A}(t)$ , for all  $t \geq s$ , and
- (2) **Pullback attraction:** For any nonempty subset  $B$  of  $X$ ,

$$\lim_{s \rightarrow -\infty} d_X(\Phi(t, s)B, \mathcal{A}(t)) = 0,$$

where  $d_X$  is the Hausdorff semi-distance in  $X$ .

According to (1) and (2) above, the family  $\mathcal{A}(t)$  is invariant under the system's dynamics and it attracts at each time  $t$  all compact initial subsets  $B$  from the remote past; see also Ghil, Chekroun, and Simonnet<sup>77</sup>, Fig. A.1, for a simple illustration.

## Appendix B: RANDOM DYNAMICAL SYSTEMS (RDS)

In physical systems, such as those encountered in the climate sciences, random time-dependent forcing is often present<sup>22</sup>. When that is so, it becomes necessary to model this type of systems using stochastic differential equations (SDEs)<sup>28</sup>.

In the theory of RDSs, random PBAs are known as *random attractors* and they can be constructed in an extended phase space composed of the phase space  $X$  and a probability space associated with the paths of the driving noise. A probability space  $(\Omega, \mathcal{F}, \mathbb{P})$  is a three-tuple, where  $\Omega$  is the sample space;  $\mathcal{F}$  is the event space, formulated as a  $\sigma$ -algebra; and  $\mathbb{P}$  is a probability measure on  $\mathcal{F}$ ; see<sup>28</sup> (Appendix A).

The probability space is then endowed with a time-dependent shift  $\theta_t$ . In the case of a stochastic-dynamic system driven by a Wiener process, as is the case here, this shift is defined on  $\Omega$  according to  $W_s(\theta_t\omega) = W_{t+s}(\omega) - W_s(\omega)$ <sup>28</sup>. With this mapping  $\theta_t$  in hand, the noise realization  $\omega$  evolves in time, and one can define a cocycle to describe the evolution of the state  $x$ .

A mapping  $\varphi : \mathbb{R} \times \Omega \times X \rightarrow X$  has the cocycle property when  $\varphi(t, \omega) = \varphi(t, \omega, \cdot) : X \rightarrow X$  satisfies the following conditions<sup>28</sup>:

- (i)  $\varphi(0, \omega)x = x$ , for all  $x \in X$  and  $\omega \in \Omega$ , and
- (ii)  $\varphi(t+s, \omega) = \varphi(t, \theta_s(\omega)) \circ \varphi(s, \omega)$ , for all  $s, t \in \mathbb{R}$  and  $\omega \in \Omega$ , where  $\circ$  denotes the composition operation for mappings of  $X$ .

Property (i) just sets the initial state of the cocycle, while property (ii) states that a cocycle is an expression of the existence and uniqueness of solutions, in the sense that going from a copy of  $X$  at time 0 to one at time  $s$  and from there on to one at time  $t + s$  is the same as going directly from 0 to  $t + s$ ; see also Ghil, Chekroun, and Simonnet<sup>77</sup>, Fig. A.2. This cocycle property is satisfied for a broad class of SDEs like those of interest here; see Arnold<sup>28</sup>.

Mathematically, given an SDE with the right properties, the probability space  $(\Omega, \mathcal{F}, \mathbb{P})$  equipped with the collections of shifts  $\theta = \{\theta_t\}_{t \in \mathbb{R}}$ , and its associated cocycle  $\varphi$ , form what is called an RDS  $(\varphi, \theta)$ , also called sometimes an RDS  $\varphi$  over  $\theta$ .

The evolution of a stochastic-dynamic system can thus be modeled by an RDS, while its associated random attractor  $\{\mathcal{A}(t; \omega)\}_{t \in \mathbb{R}}$  provides the natural extension of a PBA (as defined in Appendix A above) to the random setting in which each individual PBA depends on the specific noise realization  $\omega \in \Omega$ . The resulting family  $\bigcup_{\omega \in \Omega} \mathcal{A}(t; \omega)$  of random compact sets provides a complete description of all the system's possible states that are likely to be observed at time  $t$ .

## Appendix C: INVARIANT MEASURES

A number of interesting properties follow from the fact that the RDS  $(\theta, \varphi)$  has a random attractor. One of these is the existence of invariant measures of  $(\theta, \varphi)$ , in the sense of RDS theory. In this Appendix, we briefly clarify this notion and discuss the properties of these measures.

To do so, recall that any RDS  $(\theta, \varphi)$  generates a skew-product semiflow  $\{\Theta(t)\}_{t \geq 0}$  on  $\Omega \times X$  by the formula

$$\Theta(t)(\omega, x) = (\theta_t\omega, \varphi(t, \omega)x), \quad t \geq 0. \quad (\text{C1})$$

The cocycle property for  $\varphi$  is equivalent to the semigroup property for  $\Theta(t)$ , namely  $\Theta(t+s) = \Theta(t)\Theta(s)$ . In what follows we denote by  $\mathcal{B}$  the  $\sigma$ -algebra of Borel sets in  $X$ ; see Arnold<sup>28</sup>. We have then the following definition.

**Definition 2.** Given an RDS  $(\varphi, \theta)$ , a probability measure  $\mu$  on  $(\Omega \times X, \mathcal{F} \times \mathcal{B})$  is called an invariant measure for  $\varphi$  if it satisfies:

- (i)  $\Theta(t)\mu = \mu$ , for all  $t \in \mathbb{R}$ .
- (ii) The basic probability measure  $\mathbb{P}$  is the marginal on  $(\Omega, \mathcal{F})$  of  $\mu$ , i.e.  $\mu(E \times X) = \mathbb{P}(E)$  for any  $E \in \mathcal{F}$ .

It is known that any probability measure  $\mu$  on  $(\Omega \times X, \mathcal{F} \times \mathcal{B})$  possesses a *disintegration* or factorization<sup>28</sup>, given by a function  $(\omega, B) \mapsto \mu_\omega(B)$  from  $\Omega \times \mathcal{B}$  into the interval  $[0, 1]$  such that:

- (i) For any  $B \in \mathcal{B}$ ,  $\mu_\omega$  is  $\mathcal{F}$ -measurable;

(ii) there exists a measurable set  $\Omega'$  in  $\Omega$  such that  $\mathbb{P}(\Omega') = 1$  and  $\mu_\omega$  is a probability measure on  $(X, \mathcal{B})$  for all  $\omega$  in  $\Omega'$ ; and

(iii) for all  $f$  in  $L^1_\mu(\Omega \times X)$  we have

$$\int_{\Omega \times X} f(\omega, x) \mu(d\omega, dx) = \int_{\Omega} \left( \int_X f(\omega, x) \mu_\omega(dx) \right) \mathbb{P}(d\omega). \quad (C2)$$

The disintegration  $\mu_\omega$  is unique  $\mathbb{P}$ -almost surely and it is also called a *sample measure*; see Young<sup>61</sup>. The invariance property (i) of Definition 2 translates into  $\varphi(t, \omega) \mu_\omega = \mu_{\theta_t \omega}$ , in terms of sample measures.

When an RDS  $(\theta, \varphi)$  possesses a random compact attractor, then it supports every invariant measure, i.e.  $\mu_\omega(\mathcal{A}(\omega)) = 1$  for almost all  $\omega$  in  $\Omega$ . In this case, the sample measure possesses a useful interpretation. To understand it, recall that, roughly speaking, the random attractor  $\mathcal{A}(t; \omega)$  determines the portions of the phase space  $X$  onto which any bounded set  $B$  is mapped at time  $t$ , when  $B$  is propagated by the cocycle  $\varphi$  from a remote past, for a given noise realization  $\omega$ . The sample measure  $\mu_{\theta_t \omega}$  supported by the random attractor  $\mathcal{A}(t; \omega)$  provides, therewith, the spatio-temporal probability distributions of the portions of the phase space  $X$  occupied by the RDS, at time  $t$  and for the noise realization  $\omega$ .

For a given stochastic-dynamic system, the set of possible invariant measures is rather large. This raises the question whether a particular class of invariant measures is “naturally chosen” by the dynamics. *Physical measures* are sample measures of special interest in this respect<sup>4,22</sup>. A probability measure  $\mu$  is physical if, for any continuous observable  $\psi : X \rightarrow \mathbb{R}$ , the time average equals the ensemble average for almost all initial data  $x_0$  that lie in a Lebesgue-positive set  $B_\mu$ , called the basin of attraction of  $\mu$ ; see Chekroun, Simonnet, and Ghil<sup>4</sup>, Eq. (5).

Sinai-Ruelle-Bowen (SRB) measures<sup>60–62</sup> form a closely related class of probability measures. A probability measure  $\mu$  is an SRB measure if its conditional measures on the unstable manifolds are absolutely continuous with respect to Lebesgue measure. For many dynamical systems, the class of physical measures coincides with that of SRB measures; small differences may exist, however, between the two concepts for certain systems. Regarding the stochastic Lorenz system (1), Chekroun, Simonnet, and Ghil<sup>4</sup>, Appendix C have rigorously shown that LORA supports a random SRB measure when the Kolmogorov operator associated with (1) is hypoelliptic and its leading Lyapunov exponent is positive. Both conditions are met for the parameter values and stochastic forcing used in Eq. (1). Strong numerical evidence provided in ref.<sup>4</sup> suggests that the measure to which the point clouds used herein converge must be physical, too.

Note that the existence of an SRB measure  $\mu$  does not guarantee its uniqueness, and that two such measures  $\mu \neq \nu$  may also have different basins of attraction,  $B_\mu \neq B_\nu$ . The extensive numerical calculations in ref.<sup>4</sup> and herein have given no indication, though, of such nonuniqueness. Still, the uniqueness of LORA’s random SRB measure or of its physical mea-

sure has not been proven rigorously, to the best of the authors’ knowledge.

#### Appendix D: BraMAH Implementation

BraMAH computes the topology of point clouds whose points are locally distributed on a branched manifold. An  $m$ -manifold is a topological space with the property that each point has a neighborhood that is homeomorphic to either a full  $m$ -ball or a half  $m$ -ball, with  $m$  in  $\mathbb{N}^{19}$ . In nonlinear dynamics, an  $m$ -branched manifold is a mathematical object embedded in a phase space of dimension  $n$  ( $m \leq n$ ) that is a manifold everywhere but at the tear points of the branches<sup>18</sup>. We refer to  $m$  as the local dimension of the branched manifold.

Subsets of points of such a point cloud can be locally approximated by  $m$ -disks. This decomposition into point subsets or “patches” is called “patch decomposition”<sup>3</sup>. A BraMAH complex is a cell complex constructed so that each patch is associated with a cell in the complex.

To define cell complexes in general, we start with a single cell. A cell of dimension  $k$  ( $k$  in  $\mathbb{Z}^+$ ) or  $k$ -cell is a set that can be mapped through a homeomorphism into the interior of a  $k$ -disk, so that the boundaries of the image are divided into a finite number of lower-dimensional cells, called faces. A cell complex  $\mathbb{K}$  is a finite set of cells, such that (a) their faces are also elements of the complex; and (b) the interiors of two cells never intersect.  $\mathbb{K}$  is said to be an  $h$ -complex, or to have dimension  $h$ , if its highest dimensional cell is an  $h$ -cell.

How does BraMAH construct cells from patches? One first partitions the point cloud  $\{\mathbf{x}_i \in \mathbb{R}^n : 1 \leq i \leq N\}$  into overlapping patches that are homeomorphic to the interior of an  $m$ -disk. A patch  $\{\mathbf{x}_i = (x_{i,1}, x_{i,2}, \dots, x_{i,n}), i = 1, \dots, N_c\}$  is built around a center  $\mathbf{x}_0 = (x_{0,1}, x_{0,2}, \dots, x_{0,n})$  by searching for the largest number  $N_c$  of points around  $\mathbf{x}_0$  that constitute good approximations to a Euclidean set of dimension  $m$ . In order to calculate  $N_c$ , candidate sets  $\{\mathbf{x}_i, i = 1, \dots, n_c\}$  are computed with its elements sorted by distance from  $\mathbf{x}_0$ , and with  $N_{\min} < n_c < N_{\max}$ . Given a candidate set, the points  $\mathbf{x}_i$  within the ball with center  $\mathbf{x}_0$  and radius  $r$  are represented by the neighborhood matrix  $X \in \mathbb{R}^{n_c \times n}$ :

$$X_{i,j} = \frac{1}{n_c^{1/2}} (x_{i,j} - x_{0,j}).$$

A local coordinate system centered at  $\mathbf{x}_0$  is provided by the singular vectors of  $X$ , with the singular values describing the distribution of the points inside the ball centered at  $\mathbf{x}_0$ . For a patch that is approximately lying on an  $m$ -disk in  $\mathbb{R}^n$ , the local singular spectrum of  $X$  has  $m$  singular values that scale linearly with  $n_c$  as  $r$  is increased. This property holds while the effects of the manifold’s curvature are negligible<sup>19,78</sup>. The remaining  $(n - m)$  singular values, which measure the deviation from the tangent space, will scale as  $r^\ell$  with  $\ell \geq 2$ .

Using this rule, the  $m$  relevant singular values and vectors that span the tangent space approximating the patch under consideration can be identified. The value of  $N_c$  is obtained when the  $m$  relevant singular values — as functions of  $n_c$

subject to  $N_{\min} < n_c < N_{\max}$  — exhibit the best linear regression coefficient.

This rule is applied repetitively until every point of the point cloud belongs to at least one patch. The patch axes are chosen so as to favor patch overlapping, in order to keep track of the gluing prescriptions between them. Each patch is transformed into a cell by using convex hulls, and the singular vectors are used to orient each cell so that neighboring cells have the same orientation, thus resulting in the complex having a uniform orientation. A BraMAH complex is a cell complex that results from applying these steps to an  $n$ -dimensional point cloud.

The next step in the BraMAH methodology is to compute the topological properties of the cell complex obtained from the algorithm above. For any given complex, a  $k$ -chain is a linear combination of  $k$ -cells with integer coefficients. The algebra of these chains allows one to describe the connectivity of the cells at each  $k$ -level. A  $k$ -hole is a closed chain, called a  $k$ -cycle, that is not the border of any higher-dimensional cell.

Our approach uses the labeled list of 0-cells of the BraMAH complex in order to build a boundary matrix and extracts the linearly independent rows of it. Then, it computes the null spaces of the transpose of the boundary matrix and expresses the  $k$ -borders in terms of the  $k$ -cycles to determine which  $k$ -cycles are homological to others. The  $k$ -cycles that are homologically independent are appended to  $H_k$ . The integer multiples found in the chain that sums up all the  $k$ -borders of the complex are used to form the orientability chain.

The results of this final phase of the method are the homology groups of the BraMAH complex expressed in terms of their generators  $\{H_k : k = 0, \dots, h\}$ , spelled out in terms of the 0-cells.

The advantages of the BraMAH methodology over PH methods are the following:

- (i) A BraMAH cell complex has two particular features: it is uniformly oriented (allowing for the computation of orientability chains) and has a dimension  $h$  agreeing with the local dimension  $m$  of the branched manifold, which is computed locally using the neighborhood matrix  $X$  (no cells with unnecessarily high dimensions are created);
- (ii) the number of  $h$ -cells is significantly lower than the number of points in the original point cloud and the complex they form is thus much easier to study, while other cell complex construction rules produce complexes with numbers of  $h$ -cells that vastly outnumber the number of points in the point cloud;
- (iii) the 0-cells of the BraMAH complex are associated with a set of points whose coordinates are identified in the original point cloud; these coordinate values can be used to embed the complex in phase space and to ascertain the mutual organization of the branched manifold's branches;
- (iv) the  $k$ -holes and orientability chains of the complex can be superimposed on the point cloud or, if  $n > 3$ , on a projection of the point cloud, allowing one to identify the branches, as well as the torsions or twists along them.

## REFERENCES

- 1 R. F. Williams, "Expanding attractors," *Publ. Math. Inst. Hautes Études Sci.* **43**, 169–203 (1974).
- 2 J. Birman and R. F. Williams, "Knotted periodic orbits in dynamical systems i: Lorenz's equations," *Topology* **22**, 47–82 (1983).
- 3 D. Sciamarella and G. B. Mindlin, "Topological structure of chaotic flows from human speech data," *Phys. Rev. Lett.* **82**, 1450 (1999).
- 4 M. D. Chekroun, E. Simonnet, and M. Ghil, "Stochastic climate dynamics: Random attractors and time-dependent invariant measures," *Phys. D* **240**, 1685–1700 (2011).
- 5 W. Thomson (Lord Kelvin), "II. On vortex atoms," *London, Edinburgh Dublin Philos. Mag. J. Sci.* **34**, 15–24 (1867).
- 6 D. S. Silver, "Knot theory's odd origins," *Am. Sci.* **94**, 158–165 (2006).
- 7 W. P. Thurston, *The Geometry and Topology of Three-manifolds* (Princeton University Princeton, NJ, 1979).
- 8 H. K. Moffatt, "Some developments in the theory of turbulence," *J. Fluid Mech.* **106**, 27–47 (1981).
- 9 R. L. Ricca and M. A. Berger, "Topological ideas and fluid mechanics," *Phys. Today* **49**, 28–34 (1996).
- 10 E. Witten, "Quantum field theory and the Jones polynomial," *Comm. Math. Phys.* **121**, 351–399 (1989).
- 11 G. A. Glatzmaier and P. H. Roberts, "A three-dimensional self-consistent computer simulation of a geomagnetic field reversal," *Nature* **377**, 203–209 (1995).
- 12 H. Kedia, I. Bialynicki-Birula, D. Peralta-Salas, and W. M. Irvine, "Tying knots in light fields," *Phys. Rev. Lett.* **111**, 150404 (2013).
- 13 H. K. Moffatt, "The degree of knottedness of tangled vortex lines," *J. Fluid Mech.* **35**, 117–129 (1969).
- 14 H. K. Moffatt, "Helicity and singular structures in fluid dynamics," *Proc. Natl. Acad. Sci.* **111**, 3663–3670 (2014).
- 15 H. Poincaré, "Analysis situs," *J. Éc. Polythec. Mat.* **1**, 1–121 (1895).
- 16 A. Hatcher, *Algebraic Topology* (Cambridge University Press, 2002).
- 17 G. M. Mindlin and R. Gilmore, "Topological analysis and synthesis of chaotic time series," *Phys. D* **58**, 229–242 (1992).
- 18 R. Gilmore, "Topological analysis of chaotic dynamical systems," *Rev. Mod. Phys.* **4**, 1455 (1998).
- 19 M. Muldoon, R. MacKay, J. Huke, and D. Broomhead, "Topology from time series," *Phys. D* **65**, 1–16 (1993).
- 20 P. Holmes and R. F. Williams, "Knotted periodic orbits in suspensions of Smale's horseshoe: torus knots and bifurcation sequences," *Arch. Ratio. Mech. Anal.* **90**, 115–194 (1985).
- 21 M. Ghil, "A century of nonlinearity in the geosciences," *Earth Space Sci.* **6**, 1007–1042 (2019).
- 22 M. Ghil and V. Lucarini, "The physics of climate variability and climate change," *Rev. Mod. Phys.* **92**, 035002 (2020).
- 23 D. Kondrashov, M. D. Chekroun, and M. Ghil, "Data-driven non-Markovian closure models," *Phys. D* **297**, 33–55 (2015).
- 24 J. Berner, U. Achatz, L. Batte, L. Bengtsson, A. Cámara, H. M. Christensen, M. Colangeli, D. R. B. Coleman, D. Crommelin, S. I. Dolaptchiev, *et al.*, "Stochastic parameterization: Toward a new view of weather and climate models," *Bull. Am. Meteorol. Soc.* **98**, 565–588 (2017).
- 25 M. D. Chekroun, H. Liu, and J. C. McWilliams, "The emergence of fast oscillations in a reduced primitive equation model and its implications for closure theories," *Comput. Fluids* **151**, 3–22 (2017).
- 26 M. Santos Gutiérrez, V. Lucarini, M. D. Chekroun, and M. Ghil, "Reduced-order models for coupled dynamical systems: Data-driven methods and the Koopman operator," *Chaos* **31**, 053116 (2021).
- 27 H. Crauel and F. Flandoli, "Attractors for random dynamical systems," *Probab. Theory Relat. Fields* **100**, 365–393 (1994).
- 28 L. Arnold, *Random Dynamical Systems* (Springer, 1988).
- 29 F. J. Romeiras, C. Grebogi, and E. Ott, "Multifractal properties of snapshot attractors of random maps," *Phys. Rev. A* **41**, 784 (1990).
- 30 E. N. Lorenz, "Deterministic nonperiodic flow," *J. Atmos. Sci.* **20**, 130–141 (1963).
- 31 J. Guckenheimer and P. Holmes, *Nonlinear Oscillations, Dynamical Systems and Bifurcations of Vector Fields*, 2nd ed. (Springer-Verlag, Berlin/Heidelberg, 1983).
- 32 M. Ghil and S. Childress, *Topics in Geophysical Fluid Dynamics: Atmo-*

*spheric Dynamics, Dynamo Theory, and Climate Dynamics* (Springer, 1987, reissued, 2012).

<sup>33</sup>D. Sciamarella and G. B. Mindlin, "Unveiling the topological structure of chaotic flows from data," *Phys. Rev. E* **64**, 036209 (2001).

<sup>34</sup>F. Chazal and M. Bertrand, "An introduction to topological data analysis: fundamental and practical aspects for data scientists," *arXiv:1710.04019* (2017).

<sup>35</sup>L. Wasserman, "Topological data analysis," *Annu. Rev. Stat. Appl.* **5**, 501–532 (2018).

<sup>36</sup>J. Murugan and D. Robertson, "An introduction to topological data analysis for physicists: From LGM to FRBs," *arXiv:1904.11044* (2019).

<sup>37</sup>G. Carlsson, T. Ishkhanov, V. De Silva, and A. Zomorodian, "On the local behavior of spaces of natural images," *Int. J. Comput. Vis.* **76**, 1–12 (2008).

<sup>38</sup>D. Taylor, F. Klimm, H. A. Harrington, M. Kramár, K. Mischaikow, M. A. Porter, and P. J. Mucha, "Topological data analysis of contagion maps for examining spreading processes on networks," *Nat. Commun.* **6**, 1–11 (2015).

<sup>39</sup>L. Speidel, H. A. Harrington, S. J. Chapman, and M. A. Porter, "Topological data analysis of continuum percolation with disks," *Phys. Rev. E* **98**, 012318 (2018).

<sup>40</sup>J. M. Chan, G. Carlsson, and R. Rabadan, "Topology of viral evolution," *Proc. Natl. Acad. Sci. USA* **110**, 18566–18571 (2013).

<sup>41</sup>R. Rabadan and A. Blumberg, *Topological Data Analysis for Genomics and Evolution: Topology in Biology* (Cambridge University Press, 2019).

<sup>42</sup>M. Gameiro, Y. Hiraoka, S. Izumi, M. Kramár, K. Mischaikow, and V. Nanda, "A topological measurement of protein compressibility," *Jpn. J. Ind. Appl. Math.* **32**, 1–17 (2015).

<sup>43</sup>H. Edelsbrunner and J. Harer, "Persistent homology—a survey," *Contemp. Math.* **453**, 257–282 (2008).

<sup>44</sup>G. Carlsson, "Topological pattern recognition for point cloud data," *Acta Numer.* **23**, 289–368 (2014).

<sup>45</sup>S. Maletić, Y. Zhao, and M. Rajković, "Persistent topological features of dynamical systems," *Chaos* **26**, 053105 (2016).

<sup>46</sup>O. E. Rössler and C. Letellier, "Chaos hierarchy—A review, thirty years later," *Topology and Dynamics of Chaos: In Celebration of Robert Gilmore's 70th Birthday*, 99–124 (2013).

<sup>47</sup>K. Strommen, M. Chantry, J. Dorrington, and N. Otter, "A topological perspective on regimes in dynamical systems," *arXiv preprint arXiv:2104.03196* (2021).

<sup>48</sup>J. G. Charney and J. G. DeVore, "Multiple flow equilibria in the atmosphere and blocking," *J. Atmos. Sci.* **36**, 1205–1216 (1979).

<sup>49</sup>M. Ghil and A. W. Robertson, "'Waves' vs. 'particles' in the atmosphere's phase space: A pathway to long-range forecasting?" *Proc. Natl. Acad. Sci. USA* **99**, (Suppl. 1), 2493–2500 (2002).

<sup>50</sup>A. Hannachi, D. M. Straus, C. L. E. Franzke, S. Corti, and T. Woollings, "Low-frequency nonlinearity and regime behavior in the Northern Hemisphere extratropical atmosphere," *Rev. Geophys.* **55**, 199–234 (2017).

<sup>51</sup>M. Ghil, A. Groth, D. Kondrashov, and A. W. Robertson, "Extratropical sub-seasonal-to-seasonal oscillations and multiple regimes: The dynamical systems view," in *The Gap Between Weather and Climate Forecasting: Sub-Seasonal to Seasonal Prediction*, edited by A. W. Robertson and F. Vitart (Elsevier, Amsterdam, The Netherlands, 2018) Chap. 6, pp. 119–142.

<sup>52</sup>A. W. Robertson and F. Vitart, eds., *The Gap Between Weather and Climate Forecasting: Sub-Seasonal to Seasonal Prediction* (Elsevier, Amsterdam, 2018).

<sup>53</sup>M. Ghil, P. L. Read, and L. A. Smith, "Geophysical flows as dynamical systems: the influence of Hide's experiments," *Astron. Geophys.* **51**, 4.28–4.35 (2010).

<sup>54</sup>G. D. Charó, G. Artana, and D. Sciamarella, "Topology of dynamical reconstructions from Lagrangian data," *Phys. D* **405**, 132371 (2020).

<sup>55</sup>V. De Silva and R. Ghrist, "Coverage in sensor networks via persistent homology," *Algebr. Geom. Topol.* **7**, 339–358 (2007).

<sup>56</sup>B. Deng, "Constructing homoclinic orbits and chaotic attractors," *Int. J. Bifurcation Chaos Appl. Sci. Eng.* **4**, 823–841 (1994).

<sup>57</sup>L. C. Kinsey, *Topology of Surfaces* (Springer, 1997).

<sup>58</sup>F. J. Romeiras, C. Grebogi, and E. Ott, "Multifractal properties of snapshot attractors of random maps," *Phys. Rev. A* **41**, 784 (1990).

<sup>59</sup>G. Drótós, T. Bódai, and T. Tél, "Probabilistic concepts in a changing climate: A snapshot attractor picture," *J. Climate* **28**, 3275–3288 (2015).

<sup>60</sup>J.-P. Eckmann and D. Ruelle, "Ergodic theory of chaos and strange attractors," *Rev. Mod. Phys.* **57**, 617–656 (1985).

<sup>61</sup>L.-S. Young, "What are SRB measures, and which dynamical systems have them?" *J. Stat. Phys.* **108**, 733–754 (2002).

<sup>62</sup>L.-S. Young, "Generalizations of SRB measures to nonautonomous, random, and infinite dimensional systems," *J. Stat. Phys.* **166**, 494–515 (2017).

<sup>63</sup>A. W. Robertson and F. Vitart, eds., *The Gap Between Weather and Climate Forecasting: Sub-Seasonal to Seasonal Prediction* (Elsevier, 2018).

<sup>64</sup>M. Ghil, "Hilbert problems for the climate sciences in the 21st century—20 years later," *Nonlinear Process. Geophys.* **27**, 429–451 (2020).

<sup>65</sup>V. Lucarini and A. Gritsun, "A new mathematical framework for atmospheric blocking events," *Clim. Dyn.* **54**, 575–598 (2020).

<sup>66</sup>P. Ashwin, S. Wieczorek, R. Vitolo, and P. Cox, "Tipping points in open systems: bifurcation, noise-induced and rate-dependent examples in the climate system," *Philos. Trans. R. Soc. A* **370**, 1166–1184 (2012).

<sup>67</sup>T. Tél, T. Bódai, G. Drótós, T. Haszpra, M. Herein, B. Kaszás, and M. Vincze, "The theory of parallel climate realizations," *J. Stat. Phys.* **179**, 1496–1530 (2020).

<sup>68</sup>S. Pierini, M. Ghil, and M. D. Chekroun, "Exploring the pullback attractors of a low-order quasigeostrophic ocean model: The deterministic case," *J. Climate* **29**, 4185–4202 (2016).

<sup>69</sup>S. Pierini, M. D. Chekroun, and M. Ghil, "The onset of chaos in nonautonomous dissipative dynamical systems: a low-order ocean-model case study," *Nonlinear Process. Geophys.* **25**, 671–692 (2018).

<sup>70</sup>M. D. Chekroun, M. Ghil, and J. D. Neelin, "Pullback attractor crisis in a delay differential ENSO model," in *Advances in Nonlinear Geosciences*, edited by A. A. Tsoris (Springer Science & Business Media, 2018) pp. 1–33.

<sup>71</sup>S. Pierini and M. Ghil, "Tipping points induced by parameter drift in an excitable ocean model," *Sci. Rep.* **11**, 1–14 (2021).

<sup>72</sup>S. Vannitsem, J. Demaeyer, and M. Ghil, "Extratropical low-frequency variability with ENSO forcing: A reduced-order coupled model study," *J. Adv. Model. Earth Syst.* , e2021MS002530 (2021), [arXiv:2103.00517v1 \[physics.ao-ph\]](https://arxiv.org/abs/2103.00517v1).

<sup>73</sup>IPCC, *Climate Change 2007 - The Physical Science Basis: Working Group I Contribution to the Fourth Assessment Report of the IPCC*, edited by S. Solomon et al. (Cambridge University Press, Cambridge, UK and New York, NY, USA, 2007).

<sup>74</sup>G. D. Charó, M. D. Chekroun, D. Sciamarella, and M. Ghil, "Topological snapshot analysis of the Lorenz convection model's random attractor," *StatPhys* **27** (2019), poster.

<sup>75</sup>G. D. Charó, M. D. Chekroun, D. Sciamarella, and M. Ghil, "Topological effects of noise on nonlinear dynamics," *eprint arXiv:2010.09611* (2020).

<sup>76</sup>T. Carvalho, G. Łukaszewicz, and J. Real, "Pullback attractors for asymptotically compact non-autonomous dynamical systems," *Nonlinear Anal.* **64**, 484–498 (2006).

<sup>77</sup>M. Ghil, M. D. Chekroun, and E. Simonnet, "Climate dynamics and fluid mechanics: Natural variability and related uncertainties," *Phys. D* **237**, 2111–2126 (2008).

<sup>78</sup>D. S. Broomhead, R. Jones, and G. P. King, "Topological dimension and local coordinates from time series data," *J. Phys. A* **20**, L563 (1987).